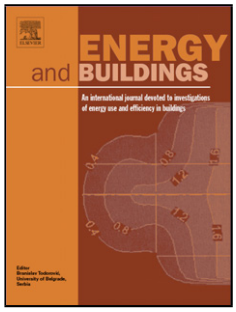


Title: Model-Based Predictive Control for Building Energy Management I: Energy Modeling and Optimal Control

Author: Saran Salakij Na Yu Samuel Paolucci Panos Antsaklis

PII: S0378-7788(16)30890-8
DOI: http://dx.doi.org/doi:10.1016/j.enbuild.2016.09.044
Reference: ENB 7033

To appear in: *ENB*

Received date: 7-3-2016
Revised date: 4-8-2016
Accepted date: 20-9-2016

Please cite this article as: Saran Salakij, Na Yu, Samuel Paolucci, Panos Antsaklis, Model-Based Predictive Control for Building Energy Management I: Energy Modeling and Optimal Control, *<![CDATA[Energy & Buildings]]>* (2016), http://dx.doi.org/10.1016/j.enbuild.2016.09.044

# Model-Based Predictive Control for Building Energy Management I: Energy Modeling and Optimal Control

Saran Salakij[a], Na Yu[b], Samuel Paolucci[b], Panos Antsaklis[c]

[a] *Department of Mechanical Engineering, Faculty of Engineering, Chulalongkorn University, Bangkok, Thailand 10330*
[b] *Department of Aerospace and Mechanical Engineering, University of Notre Dame, Notre Dame, IN 46556*
[c] *Department of Electrical Engineering, University of Notre Dame, Notre Dame, IN 46556*

**Abstract**

The simultaneous heat and moisture transfer in the building envelope has an important influence on the indoor climate and the overall thermal performance of buildings. In this work, the development of a Building Energy Analysis Model (BEAM) predicting whole building heat and moisture transfer is presented. The coupled heat and moisture transfer model takes into account most of the main hygrothermal effects in buildings. The coupled system model is implemented in Matlab, and verified with EnergyPlus. Furthermore, BEAM is reduced via a physically based model order reduction to a lower order system model (Re-BEAM) to be easily integrated with a control algorithm. By utilizing Re-BEAM, a Model-Based Predictive Control (MBPC) method is developed to incorporate critical building information into control algorithms, such that the building energy consumption is minimized while comfort conditions are maintained. The resulting optimal setpoint schedule can be applied on any HVAC system. Simulation results of a building structure demonstrate the superiority in terms of energy and peak load reductions compared with traditional constant control methods and control methods that use a occupants-varying temperature schedule.

*Keywords:*
Building energy model, energy efficiency, thermal model, hygrothermal model, model-based control

## 1. Introduction

According to the United Sates Green Building Council [1], buildings account for 40% of domestic primary energy consumption, 36% of natural gas use, and 72% of U.S. electricity usage. Therefore the energy savings related to buildings are significant objectives of many research groups, among which, implementing advanced control strategies in the building control system is one of the most popular approaches. Two main research directions are pursued in advanced control of building energy management of Heating, Ventilation, and Air Conditioning (HVAC) systems: learning-based methods of artificial intelligence and Model-Based Predictive Control (MBPC).

Learning-based methods include genetic algorithms, fuzzy techniques, and neural networks [2]. The advantage of these methods is that they do not need to know detailed physical information of the system. It is easier to be implemented when many on-site measurements are available, but the subsequent optimization process is not easy since it lacks physical insights and does not deal well with disturbances caused by varying occupants' behaviors or physical changes in a building. Also, the model accuracy depends substantively on the space-resolution of the on-site measurements. Popularly used smart thermostats in the current market, for example, Honeywell [3] and Ecobee [4], are based on simple logic to take control actions at specific times, and NEST [5] is integrated with machine learning methods to learn occupants' schedule patterns. Such approach has proven to improve a building's energy efficiency.

MBPC uses a model to predict the future state evolution of the system and generates a vector of control actions that minimize a certain cost function over the prediction horizon (the prediction time period in the future) in the presence of external disturbances and constraints. It can be regarded as a type of optimal control that is based on a mathematical model with knowledge of the building system. It employs weather and occupancy information to implement optimization in control strategies as a means to minimize the energy consumption, while ensuring comfort conditions. Compared with conventional control methods applied to building climate control, MBPC stands out for its superior performance with lower energy consumption, better transient response, and consistent performance under varying conditions [6]. Shaikh et al. [7] summarized and categorized 121 works on the state-of-the-art intelligent control systems for energy and comfort management in smart energy buildings in terms of building types, different control and optimization methods, and also discussed advantages of the MBPC method over other conventional control methods. Privara et al. [8] show that using dynamic modeling in building climate control can lead to the largest reduction of energy consumption. Knowing the physical information of a building has many advantages: more accurate calculations of thermal loads, possibilities to implement control actions on windows and doors, detect possible structure damages that may undermine the buildings' energy efficiency, and also allow pre-cooling or pre-heating of rooms by taking advantage of a building's thermal capacitance to reduce energy consumption and peak loads. Much research

work has been done to show good energy efficiency by using MBPC. Maasoumy et al. [9] presented a model based hierarchical control strategy that balances comfort and energy consumption, and showed that the proposed MBPC saves 67.3% total airflow compared with the regular controller used in the building. Aswani et al. [10] combined a mathematical model of room temperature with statistical methods to compute the heating loads due to occupants and equipment, and a learning-based model-predictive control method was used to learn and compensate for the amount of heating due to varying occupancy. Based on a physical thermal model of the building, Odlewurtel et al. [11] developed a stochastic model predictive control (SMPC) strategy for building climate control that takes into account the uncertainty due to the use of weather predictions, and showed that SMPC outperforms current control practices based on the results of a large-scale simulation of one room. Amini et al. [12] used a two stage Mixed Integer Linear Programming to solve the residential energy scheduling optimization problem, considering the customer preferences and appliances specifications, and evaluated the effectiveness of the proposed model in terms of cost savings by considering three appliances and four pricing schemes. Schmelas et al. [13] presented an adaptive and predictive computational method based on multiple linear regressions for control, and demonstrated the practicality in application and saving of computational time by implementing experiments on a two room model. Ascione et al. [14] proposed a simulation-based model predicitve control, which combines EnergyPlus and MATLAB. The goal was to optimize the hourly temperature setpoint based on weather forecast and occupancy profiles. Also it used a reliable minimum run period to overcome the issue of large computational times.

Reliable predictions from an identified energy model of a building are crucial for the effective performance of MBPC. Commonly used building energy modeling tools (e.g., EnergyPlus [15], DOE [16], TRANSYS [17], ESP-r [18]) are designed primarily for evaluating the energy use of existing buildings, but not for integrating real-time control algorithms due to the complexity of those tools [19]. Therefore, it is significant to establish a simple but relatively accurate energy model for a building so that it provides a satisfactory predicted system dynamics. Based on substantial work that has been done on building modeling, three approaches are generally used: mathematical models ("white box"), data driven models ("black box"), and hybrid models [20, 21]. White box means the physical properties of a building are known and governing equations are established to simulate the thermal performance of a building. The lumped capacitance and Computational Fluid Dynamics (CFD) models are two examples. Black box means that no information regarding the building is required, and correlations between building energy consumption and operational data is established by using statistical information. Hybrid models combine mathematical and data driven models.

The present work aims at developing a model-based predictive control for a typical building's HVAC system. In order to achieve this, a predictive energy model of a residential building is developed and used to implement an optimized desired schedule of temperature and humidity based on occupancy schedule and outdoor environmental conditions. Experimental validations of the developed model and the energy-saving benefit are demonstrated in Part II [22].

## 2. Building hygrothermal model

A Building Energy Analysis Model (BEAM) is developed as a physically based model to simulate dynamics of both temperature and humidity of indoor air in a residential building for energy management. In general, the building can be viewed as an assembly of spaces, representing rooms, and surfaces, representing walls. Doors and windows are considered as parts of surfaces, which allow air to transport across the surface when they are opened. Common heat and moisture transfer mechanisms related to a wall are illustrated in Fig. 1. It includes conduction within a wall, convection at each surface, and irradation. To obtain the results, BEAM requires the inputs from a building system, such as the geometry information, construction information, system components, and weather conditions. Instead of using the IDF file format commonly used in other energy simulation program such as EnergyPlus, BEAM uses the gbXML file format that can be exported directly from Autodesk Revit Architecture [23], which is one of the dominant Building Information Modeling (BIM) tools commonly used by architects. Without necessity of file conversion, the gbXML file looses less geometry information compared with a converted IDF file. BEAM is used to estimate hygrothermal interactions between physically connected spaces and other time-dependent conditions such as weather conditions (e.g., outdoor temperature, relative humidity, wind, and solar irradiation). Two types of solar irradiation, accounting for shading effects, are considered: direct and diffusive. Details regarding the solar irradiation modeling is given in Appendix A. Apart from architectural structure and weather conditions, BEAM also accounts for occupancy schedules, internal heat sources (i.e., sensible heat from occupants and appliances), internal moisture sources (i.e., occupants breath and sweat), and state and input constraints as external inputs. Outputs are the temperatures and relative humidities of spaces and wall surfaces.

To obtain a relatively accurate but not over-complicated model, BEAM is based on a lumped capacitance 3R2C model [24–26]. The lumped capacitance 3R2C model is developed as an analogy to an electrical circuit network as shown in Fig. 1. Basically, by using lumped capacitance, the indoor air is assumed to be well-mixed and represented by one node. Each wall's surface is treated as homogeneous and represented as one node. Each node has its own thermal and moisture capacitance, and connects with other nodes through thermal and moisture resistances. Therefore, each wall would consist of three resistances (3R), one corresponding to conduction and two corresponding to convection, and two capacitances (2C) of the wall's surfaces. For a complete building, the electrical analogous circuit network, simulating a building hygrothermal model, is created based on architectural structure information, which indicates the connections among spaces, surfaces, ground and outdoor air.

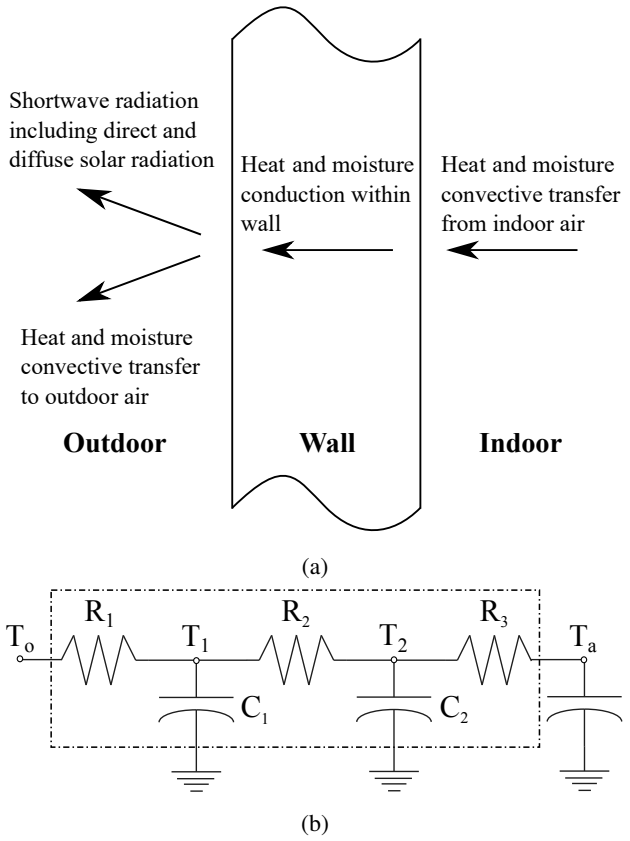


Figure 1: Heat and moisture transfer through a wall: (a) physical diagram, and (b) 3R2C analogy.

In addition to the lumped capacitance assumption, several additional assumptions are made in BEAM: (1) all opaque surfaces are diffuse and gray; (2) long wave radiation exchanges among interior wall surfaces are negligible; (3) heat and moisture transfers are one dimensional in the spaces and walls; (4) energy stored in windows is negligible; and (5) the solar radiation transmitted through windows is considered as additional heat deposited on the floor of the room. With these assumptions, governing equations for both heat and moisture transfer in spaces and walls are given a follows.

### *2.1. Governing equations for heat and moisture transfer*

To account for thermal effects caused by moisture transfer, coupled governing equations of heat and moisture are established. In addition to sensible heat generation caused by both occupants and appliances, BEAM also considers latent heat generation due to condensation occurring during moisture transfer. Ventilation and infiltration affects both temperature and relative humidity in a space as both heat and moisture are carried with the transmitted air. Estimates of ventilation and infiltration rates are given in Appendix B. Note that in this work the chosen state variable that represents moisture conditions of both air and walls is the relative humidity, since relative humidity is continuous at a wall-space interface while the humidity ratio and moisture content are not [27].

#### *2.1.1. Coupled heat and moisture transfer equations in a space*

The general governing equation describing the energy stored in moist air in a room is written as follows [28]:

$$\begin{aligned}
&\rho_a V_a \frac{d}{dt}[(c_{pa} + \omega_a c_{pv})T_a] \\
&= \sum_{i=1}^{N_{walls}} h_i A_i (T_{w,i} - T_a) \\
&+ \dot{m}_e c_{pa}(T_e - T_a) + \dot{m}_e c_{pv}(\omega_e T_e - \omega_a T_a) \\
&+ \sum_{i=1}^{N_{zones}} \dot{m}_{z,i} c_{pa}(T_{z,i} - T_a) + \sum_{i=1}^{N_{zones}} \dot{m}_{z,i} c_{pv}(\omega_{z,i} T_{z,i} - \omega_a T_a) \\
&- \dot{m}_g i_{fg}|_{T_g} + \sum_{i=1}^{N} \dot{Q}_i,
\end{aligned} \tag{1}$$

where $\rho$, $V$, $c_{pv}$, $T$, $h$, $A$, $\omega$, and $Q$ are density, volume, specific heat of water vapor, temperature, heat transfer coefficient, area, mass flow rate, humidity ratio and internal heat source, respectively. The subscripts $a$, $z$, $e$ and $w$ associated with these quantities refer to the room air, the neighboring zone, external outside air, and wall's surface, respectively. The quantity $\dot{m}_e$ represents the mass flow rate of air between the room and outside, while $\dot{m}_z$ represents the one between the considered room and the other room. These air flows are due to ventilation and infiltration. The right hand side of Eq. (1) represents convective heat transfer between air and interior wall surfaces, convective energy transfer of air and moisture due to ventilation and infiltration between indoor and outdoor as well as air exchange between zones, latent heat sink due to soft moisture sources, and internal heat sources, respectively. Notice that during moisture transport between room air and an interior wall surface, since water cannot remain in the air, condensation/evaporation occurs on the wall surface and the heat source/sink caused by the phase change is accounted in the wall surface. The term $\dot{m}_g i_{fg}|_{T_g}$ refers to heat generation caused by the moisture source in the room, such as airflow from a HVAC system. Internal heat sources, $\sum_{i=1}^{N} \dot{Q}_i$, include occupants and electronic equipment, and standard values of internal heat sources [29] are utilized.

Since the heat transfer caused by moisture transport in the wall is far smaller compared to the heat transfer caused by temperature differences, the terms that involve the humidity ratio are neglected. Equation (1) then simplifies to

$$\begin{aligned}
&\rho_{air} V_a c_{pa} \frac{dT_a}{dt} \\
&= \sum_{i=1}^{N_{walls}} h_i A_i (T_{wall,i} - T_a) + \dot{m}_e c_{pa}(T_e - T_a) \\
&+ \sum_{i=1}^{N_{zones}} \dot{m}_{z,i} C_{pa}(T_{z,i} - T_a) + \dot{m}_g i_{fg}|_{T_g} + \sum_{i=1}^{N} \dot{Q}_i.
\end{aligned} \tag{2}$$

For moisture transport in room air, the transient humidity ratio of room air is balanced by the moisture transport from internal latent loads $\dot{K}_g$, moisture convection between the room air and wall surfaces, moisture exchange through airflows between

multi-zones, and moisture transfer due to infiltration/ventilation with the outside air:

$$\begin{aligned}\rho_a V_a c_m \frac{d\omega_a}{dt} &= \dot{K}_g + \sum_{i=1}^{N_{wall}} h_{M,i} A_i (P_{v,i} - P_{v,a}) \\ &+ \sum_{i=1}^{N_{zones}} \dot{m}_i(\omega_{z,i} - \omega_a) + \dot{m}_e(\omega_e - \omega_a),\end{aligned} \tag{3}$$

where $c_m$ is the humidity capacity multiplier [30] (normally taking the value of 1), $\dot{K}_g$ is internal moisture source, which may include cooking, washing, plants, and people (for people, the averaged moisture generation is 0.18 kg/h [31]), $h_M$ is the moisture convection coefficient, and $P_v$ is the partial vapor pressure, respectively.

Particularly in air, the relative humidity $\phi_a$ can also be related to the humidity ratio $\omega_a$:

$$\phi_a = P_v/P_s = \omega_a/\omega_s, \tag{4}$$

where $P_s$ is the saturated vapor pressure, and the saturated humidity ratio, $\omega_s$, is a function of temperature [32]:

$$\omega_s = \frac{1}{R_m \rho_a T} \exp\left(23.7093 - \frac{4111}{T - 35.45}\right). \tag{5}$$

Therefore, the term $d\omega_a/dt$ in Eq. (3) can be rewritten in terms of $\phi_a$ and $\omega_s$ as:

$$\frac{d\omega_a}{dt} = \omega_s|_{T_a} \frac{\partial \phi_a}{\partial t} + \phi_a \frac{\partial \omega_s|_{T_a}}{\partial T_a} \frac{\partial T_a}{\partial t}. \tag{6}$$

Using Eqs. (4) and (6), Eq (3) can be rewritten in terms of $\phi_a$ and $T_a$ as follows:

$$\begin{aligned}\rho_a V_a c_m &\left(\omega_s|_{T_a} \frac{d\phi_a}{dt} + \phi_a \frac{d\omega_s}{dT} \frac{dT_a}{dt}\right) \\ &= \dot{K}_g + \sum_{i=1}^{N_{wall}} h_{M,i} A_i \left(\phi_{w,i} P_s|_{T_{wall,i}} - \phi_a P_s|_{T_a}\right) \\ &+ \sum_{i=1}^{N_z} \dot{m}_i \left(\phi_{z,i}\omega_s|_{T_{z,i}} - \phi_a \omega_s|_{T_a}\right) + \dot{m}_e(\phi_e \omega_s|_{T_e} - \phi_a \omega_s|_{T_a}).\end{aligned} \tag{7}$$

In summary, Eqs (2) and (7) provide the coupled relations between temperature and relative humidity of room air and wall surfaces in a building.

### *2.1.2. Coupled heat and moisture transfer equations in a wall*

The general one-dimensional heat transfer equation in a composite wall with heat generation can be written as [28]

$$\rho_m c_{pm} \frac{\partial T_m}{\partial t} = \frac{\partial}{\partial x}\left(\lambda \frac{\partial T_m}{\partial x}\right) + \dot{g}, \tag{8}$$

where $\rho_m$, $c_{pm}$ and $T_m$ are the density, the specific heat capacity and the temperature of the wall material, respectively, $\lambda$ is heat conductivity, and $\dot{g}$ is the heat source. In this case, the heat source/sink is caused by condensation/evaporation inside the wall material, which is quantified by accounting for the difference of the gradient of water vapor flux. Using Fick's law [33], the heat generation inside a wall caused by condensation/evaporation is written as

$$\dot{g} = i_{fg} \frac{\partial}{\partial x}\left(\delta_v \frac{\partial P_v}{\partial x}\right), \tag{9}$$

where $i_{fg}$ is the latent heat of condensation/evaporation, and $\delta_v$ is the vapor permeability.

To use the $3R2C$ model to develop the heat transfer equation for a wall, Eq. (8) is integrated through half of the wall volume. For simplicity, several assumptions are made. The thermal conductivity, $\lambda$, and the vapor permeability, $\delta_v$, are assumed to be constant. Condensation/evaporation are assumed to occur only on the wall surface, and the amount of condensation/evaporation due to latent heat on the wall boundary is proportional to the difference between two mass flow rates: the vapor flux in the wall from one side to the other side due to the two sides' vapor pressure difference and the vapor flux due to the vapor pressure difference between the wall surface and the air.

Boundary conditions related to heat and moisture transfers are indicated in Fig. 1a(a). On the interior side of the wall, there is heat and moisture convection between the indoor air and the interior wall surface. Within the wall, there is heat and moisture conduction. On the exterior side of the wall, there is external heat and moisture convection between the exterior wall surface and the outdoor air, and also there is solar radiation projected on the exterior wall surface. With these conditions, the heat equations of a wall are written as

$$\begin{aligned}\frac{\rho_m c_{pm} A L}{2} \frac{\partial T_{w,i}}{\partial t} &= \frac{T_{w,e} - T_{w,i}}{R_m} \\ &+ i_{fg}|_{T_{w,i}} A \left(\delta_v \frac{\phi_{w,e} P_s|_{T_{w,e}} - \phi_{w,i} P_s|_{T_{w,i}}}{L}\right) \\ &+ \dot{m}_{w,i} i_{fg}|_{T_{w,i}} + h_{w,i} A (T_{a,i} - T_{w,i}),\end{aligned} \tag{10a}$$

$$\begin{aligned}\frac{\rho_m c_{pm} A L}{2} \frac{\partial T_{w,e}}{\partial t} &= \frac{T_{w,i} - T_{w,e}}{R_m} \\ &+ i_{fg}|_{T_{w,e}} A \left(\delta_v \frac{\phi_{w,i} P_s|_{T_{w,i}} - \phi_{w,e} P_s|_{T_{w,e}}}{L}\right) \\ &+ \dot{m}_{w,e} i_{fg}|_{T_{w,e}} + h_{w,e} A (T_{a,e} - T_{w,e}) + \dot{Q}_{solar},\end{aligned} \tag{10b}$$

where $R_m$ and $L$ are the thermal resistant and the thickness of the wall material. The subscripts $i$ and $e$ refer to the interior and exterior side of a wall. Noted that for the cases where the wall is an interior wall, only Eq. (10a) is used for both sides of the walls. The term $\dot{Q}_{solar}$ accounts for the solar radiation received by an exterior wall surface or transmitted through a transparent window. The capability of a window to transmit solar radiation into the indoor air is characterized by a Solar Heat Gain Coefficient (SHGC), which is a function of the incident angle of the solar direct radiation at a specific time. The amount of solar radiation transmitted through a window is calculated by multi-

plying the total solar radiation projected on the window surface area with SHGC. More details are given by Klems [34].

The quantity $\dot{m}_w$ in Eqs. (10a) and (10b) provide the condensation/evaporation rate on a wall surface. This term only exists when the relative humidity of the wall is unity (saturated). It is evaluated by considering the moisture transport flow rate between air and a wall surface. Using Eq. (4) to rewrite $P_v$ in terms of $\phi$ and $P_s$, it can be computed from the following equation:

$$\dot{m}_w = \begin{cases} h_M A \left(\phi_a P_s|_{T_a} - P_s|_{T_{wall}}\right) & \text{if } \phi_{wall} = 1, \\ 0 & \text{if } \phi_{wall} < 1, \end{cases} \tag{11}$$

where $h_M$ is the moisture convection coefficient, which is analogous to the heat convection coefficient $h_w$. It is used to characterize the moisture transport flow rate between the wall surface and air. Based on the Chilton-Colburn analogy [35], a relation between $h_M$ and $h_w$ is given by

$$h_M = 7.1027 \times 10^{-9} h. \tag{12}$$

As most building materials are porous by nature, moisture primarily exists in pores and is transported in both liquid and vapor forms. As a result, it is necessary to also consider moisture content and moisture transport in both liquid and vapor phases within walls and ground surface.

Many studies [36–39] have been conducted to investigate the thermodynamics of moisture transport in porous materials. While in contact with moist air, hygroscopic materials adsorb water molecules at the inner surfaces of the pore system until they reach an equilibrium. The main mechanisms of moisture transport are provided by vapor diffusion and capillary suction. Vapor diffusion is described by Fick's law [33] as

$$J_v = \delta_v \frac{\partial P_v}{\partial x}, \tag{13}$$

where the driven potential is vapor pressure, $P_v$. Using Eq. (4), vapor pressure is expressed in terms of relative humidity and saturated vapor pressure. Capillary suction occurring in liquid transport is described by Darcy's law [40] as

$$J_l = D_l \frac{\partial(\Delta P_{lv})}{\partial x}, \tag{14}$$

where $D_l$ is the liquid conductivity (i.e., the ratio of permeability of material to dynamic viscosity of fluid). The suction pressure, $\Delta P_{lv}$, is the driving potential of capillary suction. By using the complete Kelvin equation [41], the gradient of suction pressure is expressed in term of the relative humidity as

$$\Delta P_{lv} = \frac{\ln \phi}{\rho_w R_v T}, \tag{15}$$

where $\rho_w$ is the density of liquid water, and $R_v$ is the specific gas constant of water vapor.

By accounting for moisture content, vapor diffusion, and capillary suction, the general one-dimensional moisture transfer equation in a composite wall can be written in terms of temperature and relative humidity [42, 43]:

$$\theta \frac{\partial \phi}{\partial t} = \frac{\partial}{\partial x}\left(D_\phi \frac{\partial \phi}{\partial x} + D_T \frac{\partial T}{\partial x}\right), \tag{16}$$

where

$$\begin{aligned} D_\phi|_{(\phi,T)} &= \delta_v P_s + \frac{D_l \rho_w R_v T}{\phi}, \\ D_T|_{(\phi,T)} &= \delta_v \phi \frac{dP_s}{dT} + D_l \rho_w R_v \ln \phi, \end{aligned} \tag{17}$$

and $\theta$ is the moisture capacity of the wall with units of $kg/m^3$. Note that $D_\phi$ and $D_T$ represent the combined liquid and vapor moisture conductivity/permeability influenced by the gradient of relative humidity, $\phi$, and temperature, $T$, respectively. List of values of the liquid conductivity, $D_l$, vapor permeability, $\delta_v$, and moisture capacity, $\theta$, of common building materials can be found in [44].

By using boundary conditions of convective moisture transfer and integrating Eq. (16) over each half-volume of the wall, the moisture governing equations for a lumped wall can be obtained in terms of relative humidity $\phi$ and temperature $T$ as

$$\begin{aligned} \frac{A L \theta_{w,i}}{2} \frac{d\phi_{w,i}}{dt} =& D_\phi|_{(\phi_{w,i},T_{w,i})} A \frac{\phi_{w,e} - \phi_{w,i}}{L} \\ &+ D_T|_{(\phi_{w,i},T_{w,i})} A \frac{T_{w,e} - T_{w,i}}{L} \\ &+ h_{M,i} A \left(\phi_{w,i} P_s|_{T_{w,i}} - \phi_{a,i} P_s|_{T_{a,i}}\right), \end{aligned} \tag{18a}$$

$$\begin{aligned} \frac{A L \theta_{w,e}}{2} \frac{d\phi_{w,e}}{dt} =& D_\phi|_{(\phi_{w,e},T_{w,e})} A \frac{\phi_{w,i} - \phi_{w,e}}{L} \\ &+ D_T|_{(\phi_{w,e},T_{w,e})} A \frac{T_{w,i} - T_{w,e}}{L} \\ &+ h_{M,e} A \left(\phi_{w,e} P_s|_{T_{w,e}} - \phi_{a,e} P_s|_{T_{a,e}}\right). \end{aligned} \tag{18b}$$

### 2.2. State-space system of BEAM

The coupled heat and moisture transfer equations are combined into a state-space system of equations, so that they can be used for optimal control. The general form of the state-space system of BEAM is written as:

$$\begin{aligned} \dot{X}(t) &= A(t)\, X(t) + B(t)\, U(t), \\ Y(t) &= C\, X(t), \end{aligned} \tag{19}$$

where $X(t)$ is a state-variable (temperature and relative humidity of indoor air and walls); $A(t)$, $B(t)$ and $C$ are the coefficient matrices; $Y(t)$ is an output (temperature and relative humidity of indoor air), and $U(t)$ is an input, which includes both uncontrollable input $U_0(t)$, such as outdoor weather conditions, and controllable input $\Delta U(t)$, such as power of the HVAC system. Note that the dimension of the controllable input $\Delta U$ usually does not match the dimension of $U$. Therefore, a transformation matrix $C_U$ is introduced such that $U = U_0 + C_U\, \Delta U$.

The critical variables related to outdoor weather conditions in the buildings' thermal performance are outdoor temperature,

relative humidity, solar radiation, wind speed, and wind direction. The climate parameters can come from three sources. The first one is from the weather database Typical Meteorological Year 3 (TMY3) [45], which is a collection of hourly typical climate data at a location, including all the important climate elements (i.e., temperature, relative humidity, solar radiation, and wind speed). The TMY3 is based on the hourly collected weather data during 1976-2005 for locations in the USA, and ones during 1991-2005 for other locations. This is used as input to BEAM for future prediction in this work. The second source is a local weather forecast, which usually only reports temperature, relative humidity, and wind speed for 5 future days. If available, this data serves as more accurate predictions of future climate variables replacing these parameters provided in the TMY3 database. The third source is any available real-time data from physical sensors, which override the parameters from the other sources.

Generally weather forecast data and weather database TMY3 are provided in the form of tables. To easily use weather data for control, the state-space system of BEAM is discretized by using the backward Euler scheme. The state-space system of BEAM in discrete form is rewritten as

$$\begin{aligned} X_{k+1} &= A_k X_k + B_k \left(U_{0,k} + C_U \Delta U_k\right), \\ Y_k &= C X_k. \end{aligned} \tag{20}$$

Note that $A_k$ and $B_k$ are time-varying coefficient matrices due to the external disturbance inputs. In practical control, these two coefficients may not be updated every time step since the weather data usually varies slowly. To decrease the computational time and improve the control efficiency, BEAM is programed such that $A_k$ and $B_k$ are updated only when weather data changes significantly more than some default tolerance values.

### 2.3. Verification of BEAM

To ensure the correctness of the implementation, a numerical solution of BEAM has been successfully compared with an analytical solution by using the Method of Manufactured Solution (MMS) [46]. In addition, BEAM has also been compared with EnergyPlus [15], which is commonly used for building energy simulations. Temperature, moisture, and monthly thermal energy consumptions are compared. Figure 2 shows the indoor air temperature and relative humidity comparisons computed from BEAM and EnergyPlus. The one room model, Model 1 shown in Fig. 3, is used, and the simulation location is Houston during August 1-8. As can be seen from Fig. 2, the results are in excellent agreement. The mean absolute difference for the indoor air temperature and relative humidity are $0.69°C$ and 1.28%, respectively. The difference in temperature may be due to the different heat transfer model used for walls. While BEAM is based on the 3R2C lumped capacitance model, EnergyPlus uses a comprehensive layer-by-layer conduction calculation. The difference in relative humidity may be due to the fact that EnergyPlus uses moisture property curves which vary with relative humidity, while BEAM uses constant properties, considering that moisture property curves are usually not easy to be obtained for most construction materials.

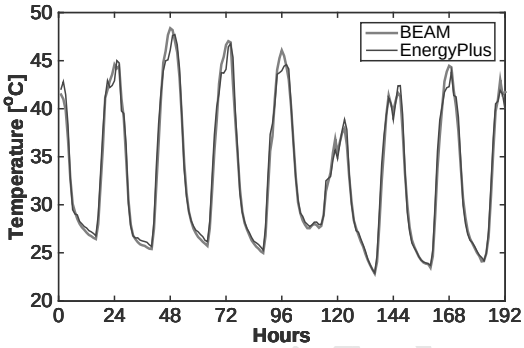


(a)

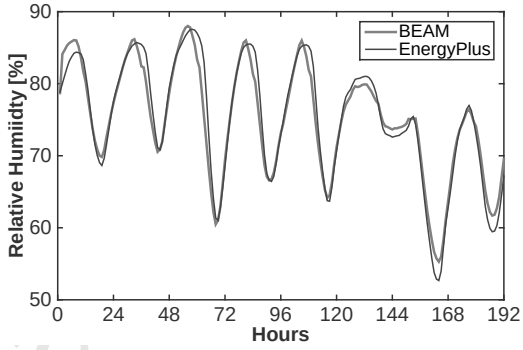


(b)

Figure 2: Indoor air temperature and relative humidity comparisons between BEAM and EnergyPlus in Houston during August 1-8.

For monthly thermal energy consumption, the three different geometric models at three different locations (Washington, DC, Emmonak, AK, and Houston, TX) are used for comparisons between BEAM and EnergyPlus. Figure 3 shows the three geometric models: one with a single room (Model 1), one with two rooms on one floor (Model 2), and one with four rooms on two floors (Model 3). Table 1 gives a detailed description of the thermal resistance, $U$, and the apparent thermal capacitance per unit area of each model, $C_a'' = \sum_{i=1}^{N} \left(\rho_{m,i} c_{pm,i} A_i\right) / \sum_{i=1}^{N} A_i$, for the buildings' materials. The Mean Relative Differences (MRD) of the predicted monthly thermal energy consumption over a year (using the weather data base TMY3) between BEAM and EnergyPlus, defined as

$$MRD = \frac{1}{12} \sum_{i_{month}}^{12} \left| \frac{E_{BEAM,i_{month}} - M_{EP,i_{month}}}{M_{EP,i_{month}}} \right|, \tag{21}$$

are shown in Table 2, where the monthly thermal energy is defined as the thermal energy used to maintain a specified indoor temperature setpoint in each geometric model for a whole month. The differences are also mainly due to the fact that BEAM uses the 3R2C lumped capacitance model while EnergyPlus uses a comprehensive layer-by-layer conduction calculation. As the 3R2C lump capacitance model simplifies calculations of walls, it is suitable for buildings with larger thermal capacitance which can better stabilize the heat transfer. Therefore, the MRDs of geometric Model 3, with a relatively com-

Table 1: Properties of the three tested geometric models.

| Type of surface | Model 1 | | Model 2 | | Model 3 | |
|---|---|---|---|---|---|---|
| | $U(W/m^2K)$ | $C_a''(J/m^2K)$ | $U(W/m^2K)$ | $C_a''(J/m^2K)$ | $U(W/m^2K)$ | $C_a''(J/m^2K)$ |
| Exterior wall | 16.7 | 8670 | 0.41 | $2.86\times10^5$ | 0.39 | $2.86\times10^5$ |
| Ground floor | 5.15 | $6.09\times10^5$ | 0.59 | $9.09\times10^5$ | 5.15 | $5.74\times10^5$ |
| Roof | 0.08 | $0.37\times10^5$ | 1.64 | $5.18\times10^5$ | 0.08 | $3.69\times10^5$ |
| Door | 3.70 | $0.25\times10^5$ | 3.70 | $0.25\times10^5$ | 2.70 | $0.25\times10^5$ |
| Window | 6.71 | $N/A$ | 6.71 | $N/A$ | 6.71 | $N/A$ |
| Interior wall | 0.39 | $2.86\times10^5$ | 0.41 | $2.86\times10^5$ | 1.28 | $0.30\times10^5$ |
| Interior floor | $N/A$ | $N/A$ | $N/A$ | $N/A$ | 0.17 | $6.09\times10^5$ |

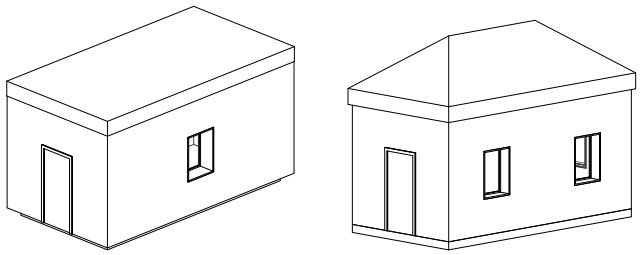

(a) Model 1



(b) Model 2

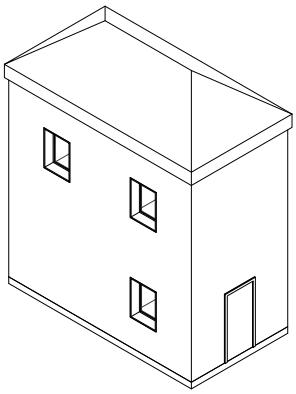

(c) Model 3

Figure 3: Three geometric models used for BEAM and EnergyPlus analysis.

plex building structure and a larger thermal capacitance, are significantly less than other two simpler structures, while for a simpler model, such as Models 1 and 2, the 3R2C simplification is amplified and thus results in an increased difference. Since the MRDs of the monthly thermal energy consumptions for all three models at the three locations are below 6.5%, we conclude that BEAM gives reasonably reliable results using a much simpler method.

Validation of BEAM is accomplished by comparing the results from the verified model with experiments. This is discussed in Part II. [22].

### *2.4. Reduced order BEAM (Re-BEAM)*

An important requirement of a dynamic model to be used for real-time control is simplicity. In general, the state-space system of BEAM consists of a pair of coupled heat and moisture transfer equations (Eqs. (2) and (3)) for each space, and coupled heat and moisture transfer equations (Eqs. (10a), (10b),

Table 2: Mean Relative Differences of the monthly thermal energy between BEAM and EnergyPlus.

| Location | Geometric model | | |
|---|---|---|---|
| | Model 1 | Model 2 | Model 3 |
| Washington, DC | 6.30% | 4.69% | 2.59% |
| Emmonak, AK | 5.00% | 2.12% | 0.96% |
| Houston, TX | 3.28% | 0.08% | 1.02% |

(18a) and (18b)) for each wall. For example, Model 3 shown in Fig. (3c) has 4 spaces and 28 surfaces. The complete dynamic model of this geometry by using BEAM consists of 64 coupled equations, and they are required to be solved simultaneously every time step. This can lead to inefficient real-time control when applying BEAM to a multi-zone building.

Many model order reduction methods have been applied to building energy modeling. One of the most commonly used is principle component analysis (PCA) or proper orthogonal decomposition (POD) methods, such as the modal analysis [47–49] and balance truncation methods [50]. Based on the demonstration by Kim and Braun [51], by applying the balance truncation method to a building energy model, the results obtained from the reduced model, consisting of 10 states, matched well with ones obtained from the 297-node full-order model of a single zone space. Another common approach to obtain a lower order model is to apply a data driven model ("black box") on simulated results from a full-order model. For example, Bualan et al. [52] used a parameter identification method to identify and optimize 5 parameters used in the proposed simplified thermal model, and proposed its integration with a model-based predicted control algorithm. Georgescu and Mezi [53] used the Koopman operator to create a lower order model from simulated results from EnergyPlus. Kim et al. [54] aggregated a linearized time-invariant (LTI) building envelope model with a LTI reduced-order indoor CFD model, obtained by performing system identification on response data generated by a commercial CFD software.

In distinction to the above methods, in this research a physically based model order reduction method, i.e., the aggregation method [55], is selected to construct the reduced order model of BEAM (Re-BEAM). The main idea of this method is to group variables that share a similar dynamic response into a single

variable. The accuracy of the reduced model depends on how the aggregated parameters and variables represent the more detailed model. Therefore, it is important to understand the physical correlations among parameters to construct an accurate reduced model. The reduced model, with the grouped parameters and variables, should be structured similar to the full-order model, but having less complexity. In other words, the interaction among individual parameters and variables are physically simplified and represented by the interaction among grouped parameters and variables. This method is directly suitable for use on detailed building model information file formats, such as gbXML, without the necessity of performing system identification on other model results. We note that an alternative popularly used method, the modal analysis method [47–49], is not applicable in this situation. The modal analysis method is usually effective for most large-scale systems. However, by the nature of this method, the fast modes in the system are usually neglected, which may eliminate crucial variables (e.g., indoor air temperature) from the energy model. Our model order reduction method gives us the flexibility to select the desired variables. The other benefit of a physically based model order reduction is that it has composability, which can be extended to be applied to a general building structure. As a result, while individual Re-BEAM models can be constructed independently, the Re-BEAM model of the connected structures can also be easily combined.

This research focuses on the systematic approach for aggregation of structure components to form a lower order model. To ensure accuracy of indoor climate control, variables related to a room's air are not aggregated. Re-BEAM is developed by aggregating all of the parameters into one for each individual room space, one for a lumped interior surface associated with each room, one for a lumped exterior surface, and one for a lumped ground surface. With $n$ the number of rooms in the considered building, the order of Re-BEAM after implementing aggregation is $2n + 2$: $n + 2$ for lumped surfaces and $n$ for room's air. Similar to an electrical circuit, the thermal and moisture capacitances of the lumped surface are evaluated as summed values of the components. Note that although the ground floor in each room is part of the interior surface of that room, it is not aggregated. Instead, the lumped ground surface is separated from the lumped interior surface since the physical time response of the ground surface is generally longer than the rest of the interior surfaces due to its relatively larger thermal capacitance. To illustrate the model order reduction, Fig. 4 shows a full-order model (BEAM) of the basic 2-room geometry, represented in Fig. (4a), and the reduced $2n+2$ order model (Re-BEAM), represented in Fig. (4b), where each continuous block represents an aggregated surface. The electrical circuit analogy, representing the full-order model and the aggregation method of the 2-room model, are shown in Fig. 5.

Simulations are performed to verify the accuracy of the Re-BEAM compared with the detailed BEAM. The three geometric models, used for the BEAM-EnergyPlus comparisons in the previous section (Models 1, 2, and 3, shown in Fig. 3), are used for comparisons. The simulations are performed for Houston, TX, and during the period of August 1-3, where outdoor temperature ranges between 22°C and 40°C, without any active temperature or humidity control. The mean absolute differences of room temperature during the three days simulation between Re-BEAM and BEAM for models 1, 2 and 3 are 0.08°C, 0.13°C and 0.23°C, respectively. As expected, the differences increase as the complexity of geometry increases. As the mean absolute differences of all the three models over the three days period are less than 0.25°C, we conclude that Re-BEAM is relatively reliable for control purposes.

It is important to note the limitation of the physical aggregation method. Although this method is a systematic model order reduction and is applicable to general building model information file formats, such as gbXML, it omits some detail information about the connection among rooms when aggregating interior walls. This lack information may be critical for cases where there are large variations among rooms' temperatures in a building such as an industrial building with a freezer room. To elaborate on this issue, consider a 3-room building. Let room B connect with room A and C, but let room A not connect with room C. In this case, the heat and moisture transferring between interior walls of room A and those of room C require the transfer through the interior walls and air of room B. With the proposed physical aggregation method, the aggregated interior wall of room A and that of room C are separated only by the aggregated interior wall of room B. As a result, heat and moisture are easier to transfer between room A and C than the real situation. This problem is minimal in common residential and commercial buildings whose range of temperature variation among rooms are usually small.

## 3. Optimal control algorithm in building energy management

The goal of implementing an energy model in a building climate control is to minimize the building's energy consumption while maintaining indoor thermal comfort for occupants. A common and effective method is to vary the desired indoor climate schedule based on the occupants' activities. The benefit of this method is that it can be applied to any setpoint-schedulable HVAC system with little or no physical modification to the system since the modification of the desired climate schedule is usually software based. By using Re-BEAM as the predictive model, and considering the occupants schedules and outdoor environmental conditions, Model Based Predictive Control (MBPC) is developed to enable optimal control strategies. In general, MBPC is performed by formulating and solving a

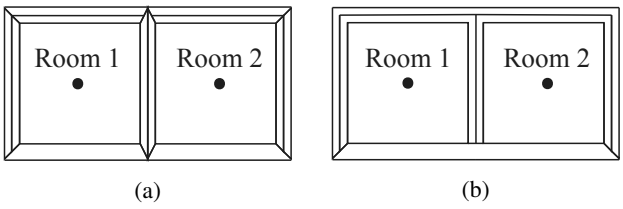


Figure 4: Schematic of basic n=2 rooms geometry components based on (a) the full-order model (BEAM), (b) the reduced $2n + 2$=6 order model (Re-BEAM).

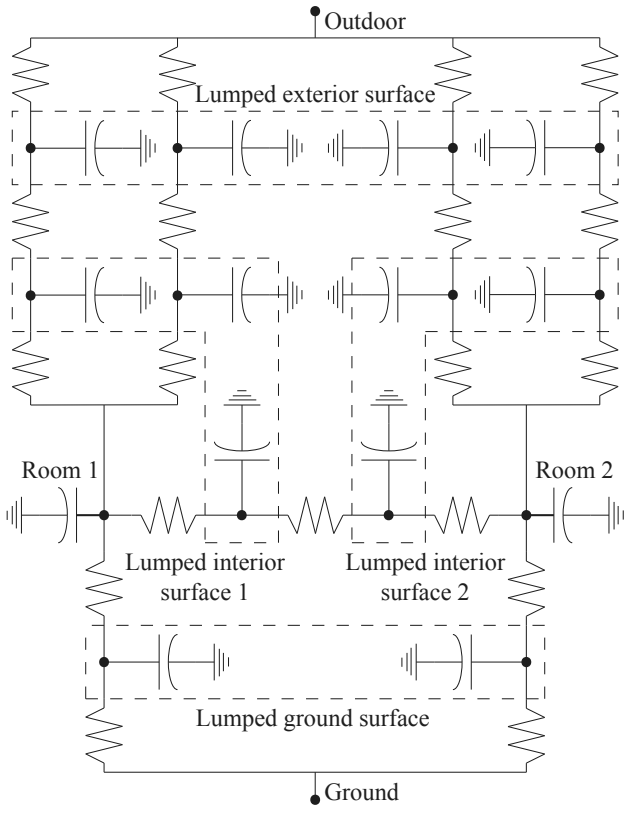


(a)

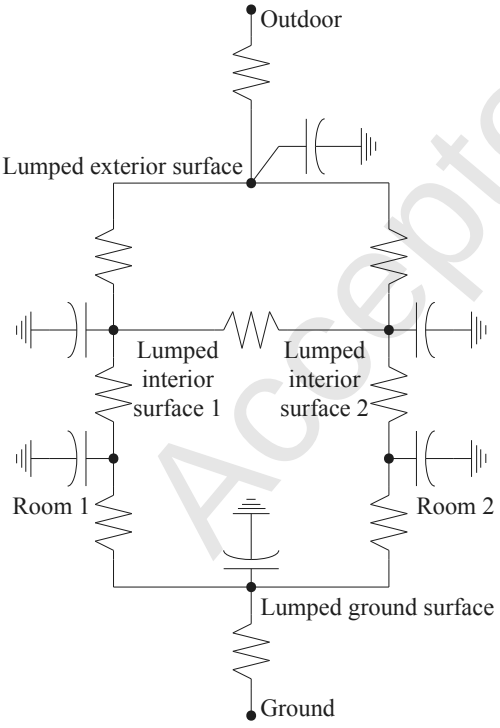


(b)

Figure 5: Electrical circuit analogy of a basic 2-room geometry based on (a) the full-order model (BEAM), and (b) the reduced $2n+2$ order model (Re-BEAM).

finite horizon optimal control problem at each sampling time interval based on the physical model. The result is a future optimal trajectory of inputs and state variables based on a cost function that satisfy both model dynamics and constraints. In this work, Re-BEAM is applied in MBPC, while the constraints on a building with given structural details are the maximum power of the HVAC system and the maximum rate of the humidifier/dehumidifier.

As the aim of optimization in a building climate control is to minimize energy consumption while maintaining thermal comfort, a quadratic formulation of the cost function is used:

$$J = \sum_{k=1}^{N} \Big[ (Y_k - r_k)^T \; W_{r,k} \; (Y_k - r_k) \Big] + \sum_{k=1}^{N-1} \Big[ (\Delta U_k)^T \; W_{\Delta U,k} \, (\Delta U_k) \Big]. \tag{22}$$

The first term of the cost function represents the cost due to the deviation of the indoor temperature and relative humidity ($Y_k$) from the reference setpoints ($r_k$). The second term represents the cost due to the power supplied by HVAC system and humidifier/dehumidifier ($\Delta U_k$). The quantities $W_{r,k}$ and $W_{\Delta U,k}$ are the weighting coefficient matrices. These weighting coefficient matrices may require to be tuned when performing MBPC so that the output reference variations are within the specified tolerance limits of comfort conditions.

The optimization algorithm is obtained by modifying the finite horizontal Linear Quadratic Tracking (LQT) [56] to account for predefined uncontrollable inputs $U_0$, which in this case includes the weather information. The optimal controllable input $\Delta U_{k-1}$ at time step $k-1$ is expressed as:

$$\Delta U_{k-1} = K^X_{k-1} \, X_{k-1} + K^{U_0}_{k-1} \, U_{0,k-1} + K^V_{k-1} \, V_k, \tag{23}$$

where $K^X_{k-1}$, $K^{U_0}_{k-1}$, and $K^V_{k-1}$ are the gains, which for a previous state-variable, $X_{k-1}$, a previous time step uncontrollable input, $U_{0,k-1}$, and a current time step reference-setpoint-related variable $V_k$, respectively. These gains are expressed as functions of the coefficient matrices $A_k$, $B_k$ and $C$ at current time step in Eq. (20), and a predicted-output-related variable $S_k$. Noted that the variables $V_k$ and $S_k$ are introduced here to indirectly include the reference setpoint $r_k$ and the predicted output $Y_k$, respectively, in the calculation for the optimal controllable input $\Delta U_k$. The gains ($K^X_{k-1}$, $K^{U_0}_{k-1}$, and $K^V_{k-1}$) are calculated backward in time starting from the last expected time step, $N$, from

$$\begin{aligned}
K^V_{k-1} &= \left( C_U^T \, B_k^T \, S_k \, B_k \, C_U + W_{\Delta U,k-1} \right)^{-1} \; C_U^T \, B_k^T, \\
K^X_{k-1} &= -\, K^V_k \, S_k \, A_k, \\
K^{U_0}_{k-1} &= -\, K^V_k \, S_k \, B_k, \\
S_{k-1} &= A_k^T \, S_k \left( A_k - B_k \, C_U \, K^X_{k-1} \right) + C^T \, W_{r,k-1} \, C, \\
V_{k-1} &= (A_k + B_k \, C_U \, S_{k-1})^T \; V_k + C^T \, W_{r,k-1} \, r_{k-1} \\
&\quad - A_k^T \, S_k \, B_k \; (I + C_U \, K_{U_0,k-1}) \; U_{0,k-1},
\end{aligned} \tag{24}$$

with initial conditions at time step $N$ of

$$S_N = C^T \, W_{r,N} \, C, \quad V_N = C^T \, W_{r,N} \, r_N. \tag{25}$$

Note that as the gains are calculated backward in time, the gains $K^V_{N-1}$, $K^X_{N-1}$, and $K^{U_0}_{N-1}$ of time step $N-1$ are required to be calculated first. However, the time-varying coefficient matrices $A_N$ and $B_N$ of either BEAM or Re-BEAM at the last expected time step cannot be easily obtained since they are also a function of the actual state variables, which have not been calculated yet. To obtained the exact values of the gains, iterations are required.

For simplicity, both time-varying coefficient matrices $A_k$ and $B_k$ in Eq. (24) are simplified by using the current time step coefficient matrices $A_1$ and $B_1$ for all time steps. In other words, the time-varying coefficient matrices $A_k$ and $B_k$ are treated as time-invariant coefficient matrices during MBPC calculation for the optimal controllable inputs. This is a reasonable estimation since both $A_k$ and $B_k$ of BEAM and Re-BEAM are usually insensitive during the period used in the MBPC for building climate control due to the large responsive timescale of the building envelope. Subsequently, the coefficient matrices $A_k$ and $B_k$ are only updated at the beginning of each MBPC calculation.

## 4. Sample results

To show the effectiveness of the proposed optimal control algorithm, the MBPC method is compared with two other common building climate control methods. The first method is a traditional constant temperature setpoint control, which is set as constant 25°C. The other control method uses a time-varying temperature setpoint schedule based on the occupants activities without applying an optimal algorithm. Typically, when occupants are sleeping the room temperature is set to be slightly lower than that when occupants are active. It should be noted that although it is unnecessary to control the room temperature when there is no occupancy, the room temperature should still be within upper and lower limits for the sake of indoor equipment conditions. In this demonstration, the room temperature setpoints during sleep, active, and away times are 25°C, 26°C and 35°C, respectively. Also, the occupancy schedule was assumed as sleeping time from 10:00 pm to 6:00 am, active time from 6:00 am to 7:00 am and 8:00 pm to 11:00 pm, and away time from 7:00 am to 8:00 pm. The MBPC method also uses the same schedule as the occupants-activities-based setpoint schedule, and then applies the optimization algorithm to obtain the optimized room temperature setpoint. The relative humidity setpoint for all three control methods is maintained constant at 40%.

The Re-BEAM simulations are performed based on a two-story residential building model located in Houston, TX during August 1-2, where the outdoor temperature ranges between 22°C and 40°C. Variation of outside weather during the two-day simulation period is obtained by interpolating the hourly weather database TMY3 using a cubic spline to obtain weather information every minute. Figure 6 shows the building model from outside and the floor plans of both stories. This building model was generated using Autodesk Revit Architecture. The dimension of the building is 8.89 m (29 ft 2 in) in length, 7.11 m (23 ft 4 in) in width, and 3.08 m (10 ft) in height for each of the two floors. The construction materials for floors, ceilings, interior, and exterior walls are 10-inch wood and 14-inch

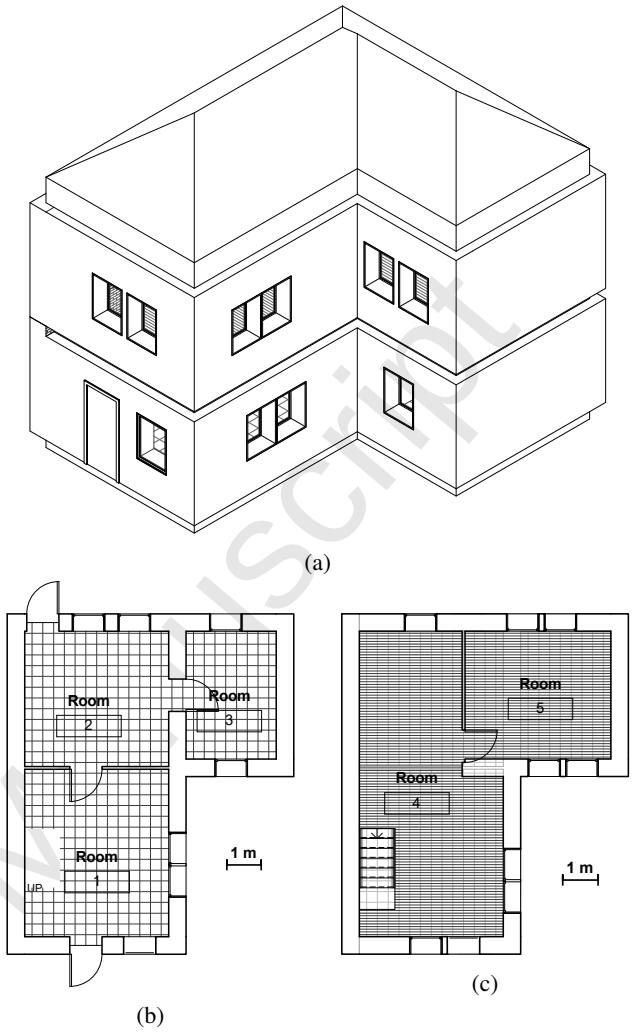


Figure 6: Geometric drawing of the sample two-story residential building showing: (a) 3-D outside view of the building, (b) the first floor plan, and (c) the second floor plan.

concrete, compound ceiling 2×4 ACT system (T-Bar Ceiling), 3 1/8-inch partition and brick. Note that these construction materials and their properties are available in the default built-in library of materials provided by Autodesk Revit Architecture.

By using the HVAC system with variable control as actuator, the thermal energy consumptions during the two-day period resulting from three different control methods are summarized in Table 3. For the HVAC system with variable control, the power supply is assumed to be able to be varied smoothly from zero to the maximum. Note that the energy consumption presented in this research is thermal energy, which is not the same as electrical energy. The proportion between those energy depends on efficiency of each HVAC system, which is not relevant in the present research. Based on the results, the MBPC method outperforms the other two methods by consuming only 57.3% of that of constant temperature setpoint control method, which consumes most energy. This demonstrates that the energy consumption of indoor climate control can be significantly improved by appropriately adjusting the temperature setpoint

schedule even without involving any hardware modification.

The differences among energy consumption results can be explained by observing the variations of rooms' temperatures and variable thermal powers provided by the HVAC system for the three different control methods. Only information of room 1 is presented in Fig. 7 and discussed as the other rooms also show similar trends. Note that the room temperature in Fig. 7(a) is not visible in the graph since it overlaps with the setpoint line. Comparing constant and varying temperature setpoint methods, Fig. 7(b) and 7(c) show that the indoor temperature during the vacancy time, i.e., when the setpoint is at 35°C, naturally rises for most of that time. On the other hand, the temperature shown in Fig. 7(a) is always maintained at 25°C during that period, which results in a large amount of unnecessary energy waste compared with the other methods, as noted in Table 3.

To explain why the MBPC method performs better than the other methods in terms of energy savings, it is necessary to closely observe Fig. 7(c). It shows that the indoor temperature changes smoothly for most of time, except during the vacant periods, and the deviation from the setpoint in other periods is less than 1°C. Compared with the result from the occupants-activities-based setpoint control method shown in Fig. 7(b), the indoor temperature resulting from the MBPC method is slightly higher. As a result, the time-average indoor temperature of the MBPC is also slightly higher, which implies lower energy consumption. It should be noted that in this demonstration the increase in indoor temperature from the setpoint when the room is occupied is less than 1°C: this means that the occupants' thermal comfort is still preserved.

The major drawback of using a varying temperature setpoint schedule is that it requires a higher peak power of the HVAC system. As seen form Fig. 7(a), the required peak power of the constant setpoint case is 880 W, which is significantly less than the other two cases. To be precise, the peak power of the MBPC case is 1990 W, while that of the occupant-activities-based setpoint case is off the graph (10300 W). This is because it requires more power to change the indoor climate condition than just maintaining it, especially when there is a sudden change in the setpoint schedule as shown in Fig. 7(b). It can be clearly seen that the peak always occurs at a transition of setpoint. By optimizing the energy consumption using the MBPC, not only there is significant improvement in energy savings, but also the method smooths the climate setpoint transition, which results in a lower peak power requirement, but still higher than that of the constant temperature setpoint case. Based on this, the maximum $\Delta U$ may require to be accounted in the cost function in future development of the optimization algorithm if the size of the HVAC system is a major concern.

Table 3: Thermal energy provided by a variable control HVAC system utilized for the sample two-story residential building located in Houston, TX during August 1-2 based on three different control methods.

| Control method | Required thermal energy $[kW \cdot h]$ | Energy-saving compared with base case |
|---|---|---|
| Constant temperature setpoint control (base case) | 166.29 | - |
| Occupant-activities-based setpoint control | 101.43 | 39.0% |
| MBPC | 95.38 | 42.6% |

It should be noted that the optimal controllable input $\Delta U_k$ obtained from Eq. (23), which is the variable input, can theoretically be applied directly to a HVAC system with variable control, such as an inverter compressor HVAC, without necessity of physical modification. This can be achievable by controlling air flow through a Fan Coil Unit (FCU) and power of the inverter compressor, such that the supplied cooling/heating power matches the specified optimal controllable input $\Delta U_k$. However, practically this cannot be easily applied. In general, the predictive optimal states obtained from the model Re-BEAM and optimal controllable input $\Delta U_k$ is used as the optimal desired setpoint schedules of temperature and humidity for the HVAC system. As a result, this approach is applicable to any HVAC system, both variable control and on/off configurations, if its control system allows input of a setpoint schedule.

To show the versatility of our approach, simulations were also performed for a traditional on/off control HVAC system with a cooling capacity of 1000 W for rooms 1, 2, and 3, and 2000 W for rooms 4 and 5 to ensure that the benefit of the MBPC also applies for a general on/off control HVAC system. The cooling capacity of HVAC systems in rooms 4 and 5 are larger than ones in rooms 1, 2 and 3 because the rooms on the second floor (rooms 4 and 5) received more heat load from the solar radiation as their ceilings are connected to the roof. As it is operated in an on/off manner, the room temperature cannot follow the temperature schedule as well as a variable control HVAC system. The allowable temperature band of ±1°C around the temperature setpoint was assumed for on/off control, which is the same default range of many commercial thermostats, e.g., Honeywell [3]. This is introduced as a means of preventing frequent chattering and also prolonging the operating life of a HVAC system. For simplicity, the power provided by the HVAC system is assumed to be either zero or the maximum (1000 W for the rooms on the first floor and 2000 W for the rooms on the second floor).

Table 4 summarizes the overall thermal energy consumptions of the 1000 W on/off control HVAC system that controls the climate in the two-stories residential building model in Houston, TX, during August 1-2 based on the three different control methods. Variations of room 1's temperature and HVAC system on/off status are shown in Fig. 8. Similar to the results from the variable control HVAC system, the MBPC performs the best among the three observed methods. Therefore, it is concluded that the MBPC for thermal control is appropriate for HVAC systems with both variable and on/off control configurations. Further demonstrations of the practical application of the MBPC are experimentally investigated in the Part II [22].

Although it is not a primary aim of this research, it is interesting to note that the overall energy consumption of the on/off control HVAC system is smaller than that of the variable control. However, one cannot generally conclude that a variable

(a) Constant temperature setpoint control method.

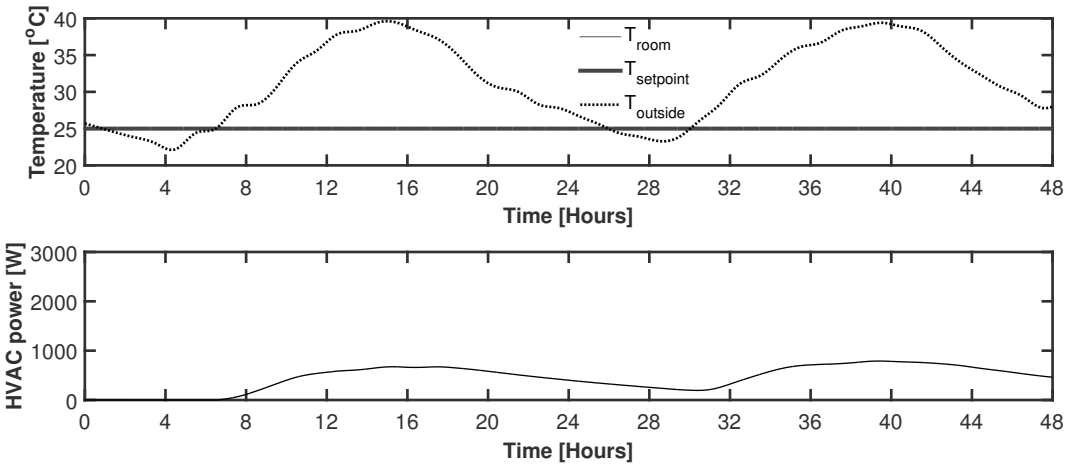


(b) Occupant-activities-based setpoint control method.

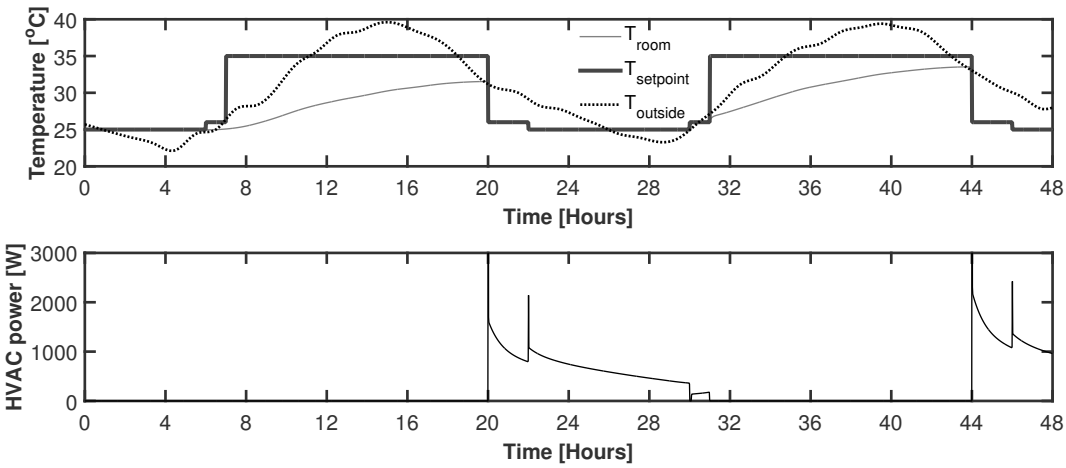


(c) MBPC method.

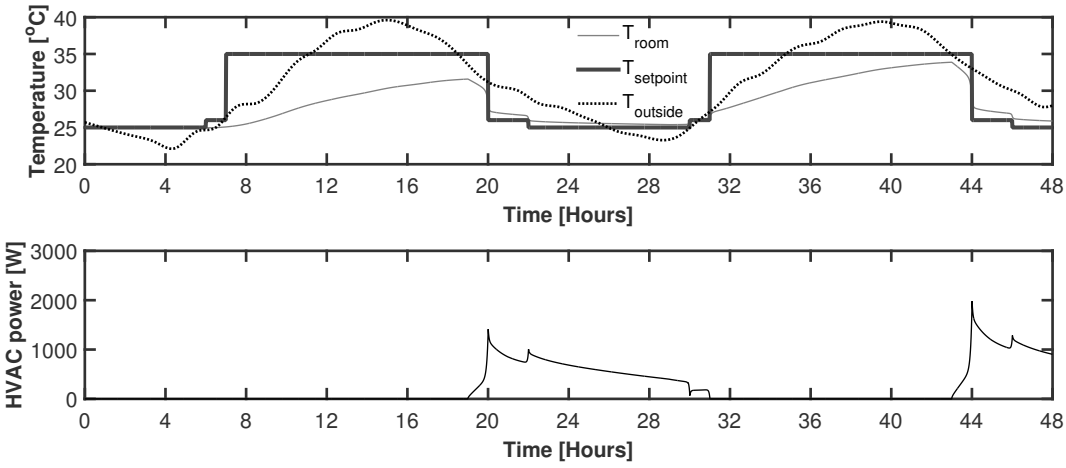


Figure 7: Simulation results of the two-story residential building model during August 1-2 in Houston, TX, showing variations of room 1's temperature and its required variable thermal power using (a) the constant temperature setpoint control method; (b) the occupant-activities-based setpoint control method (note that the off-scale two power peaks reach values of 7585 W and 10300 W.); and (c) the MBPC method.

Table 4: Thermal energy provided by 1000 W on/off control HVAC system utilized for the two-story residential building model located in Houston, TX, during August 1-2 based on three different control methods.

| Control method | Required thermal energy $[kW \cdot h]$ | Energy-saving compared with base case |
|---|---|---|
| Constant temperature setpoint control (base case) | 146.48 | - |
| Occupant-activities-based setpoint control | 96.67 | 34.1% |
| MBPC | 91.75 | 37.4% |

control HVAC system is less efficient than a traditional on/off control. This is because this study does not account for electrical energy loss during the startup process of the on/off control HVAC system. Also, the frequent on/off can damage the equipment longevity in long terms. Further investigation is required on this issue.

## 5. Conclusions

This work focuses on the development of an accurate and reliable building hygrothermal model based on a physical approach and Model-Based Predictive Control (MBPC) method to perform optimal control in building energy management. The developed BEAM was verified with an analytical solution, and compared with simulation results from EnergyPlus. To be computationally-efficient and easily integrated with a control algorithm, Re-BEAM was developed with good accuracy by reducing the order of BEAM. The MBPC was developed by applying a finite horizon Linear Quadratic Tracking (LQT) method to the model to obtain an optimized temperature setpoint schedule based on occupants' activities.

Demonstrations of applying the MBPC were performed on a residential building model by using Re-BEAM to perform the simulations. Results show that the MBPC saves thermal energy consumption up to nearly 43% compared with a traditional constant temperature setpoint control method. Further analysis shows that energy is primarily saved by varying the temperature setpoint with the occupants activities; for example, the indoor climate is maintained in comfort zone only when there is occupancy. In addition, further energy saving is obtained by smoothing temperature setpoints transitions resulting from the optimization process.

Simulation results of using MBPC on a complex building structure look promising in improving a building energy efficiency. Note that the performance of using MBPC should depend on the situation of a particular building system, such as the building materials and heating/cooling system size. In future works, the use of sensors in the building system will provide real-time measured data input to the model, where a machine-learning algorithm can be integrated with the MBPC algorithm to learn the occupants schedules and further optimize the temperature schedule. The use of Re-BEAM with other available predictive control methods should be comprehensively investigated. Experimental validations demonstrating the reliability of Re-BEAM and energy-saving benefits of applying the MBPC method are demonstrated in Part II [22].

## Acknowledgements

Financial support from the U.S. Army Natick Soldier Research, Development and Engineering Center (NSRDEC) under Contract No. W911QY-12-C-0128 is gratefully acknowledged.

## Appendix A. Solar irradiation and shading effects

For an exterior wall surface, the total received radiation $\dot{Q}_{S\,olar}$ (also named as the global horizontal radiation) includes direct normal radiation $I_{dir,n}$, diffuse horizontal radiation $I_{dif,h}$, and ground-reflected radiation. However, because ground reflected radiation is usually insignificant compared to direct and diffuse, for all practical purposes global radiation is given by the sum of direct $I_{dir,n}$ and diffuse radiation $I_{dif,h}$ only:

$$I_{total} = I_{dir,n} + I_{dif,h}. \tag{A.1}$$

The direct solar radiation represents the portion of solar energy that is transmitted directly through the atmosphere. Its direction remains basically unchanged from the time it was emitted from the sun to the time it strikes the building surface. Direct radiation can be expressed as:

$$I_{dir,n} = I_{dir} \cos\theta, \tag{A.2}$$

where the normal direct solar radiation $I_{dir}$ can be taken directly from the weather file TMY3 and $\theta$ is the solar incidence angle, which can be calculated through the following equation:

$$\cos\theta = \sin\psi_s \cos\phi_w + \cos(\psi_s - \psi_w)\cos\psi_s \sin\phi_w, \tag{A.3}$$

where $\psi_s$ is the solar azimuth angle, $\phi_w$ is the wall surface's tilted angle, and $\psi_w$ is surface azimuth angle.

Diffuse radiation is the portion of solar energy that has collided with one or more particles in the atmosphere and has been re-emitted in some new direction and can be expressed as

$$I_{dif,h} = I_{dif} \frac{1 + \cos\phi_w}{2}, \tag{A.4}$$

where the diffuse horizontal radiation $I_{dif}$ is taken directly from the TMY3 weather file.

Shading diminishes the effectiveness of irradiation. To account for this effect, the model predicts the location of a shadow cast from other surfaces onto the receiving surface, then substracts the shadow area from the total surface area resulting in the net effective irradiated area.

The process of evaluating the shading area of the considered surface is modified from that in EnergyPlus Engineering Manual [32]. In general, it can be done by evaluating the shadow casting by casting surfaces on the receiving surface. To avoid unnecessary calculation, the first step is to identify the potential shadow casting surfaces, whose part of them are above and

(a) Constant temperature setpoint control method.

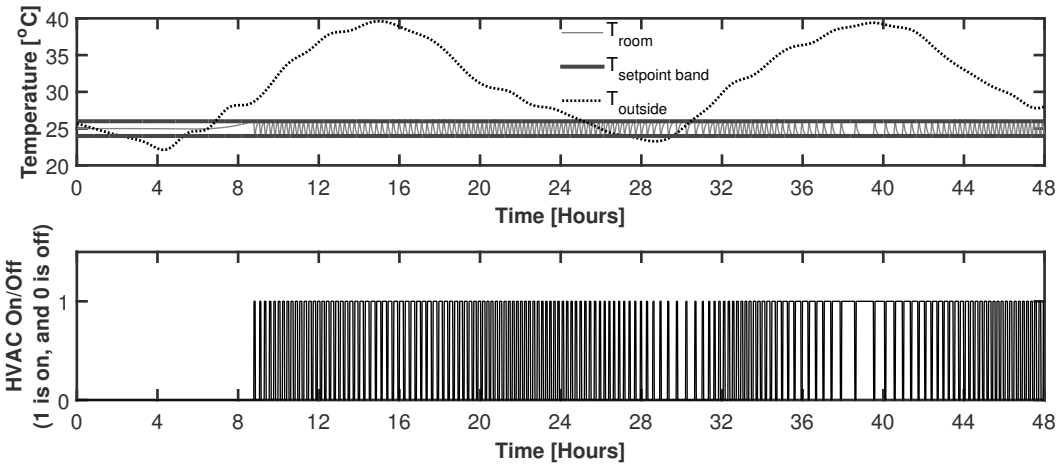


(b) Occupant-activities-based setpoint control method.

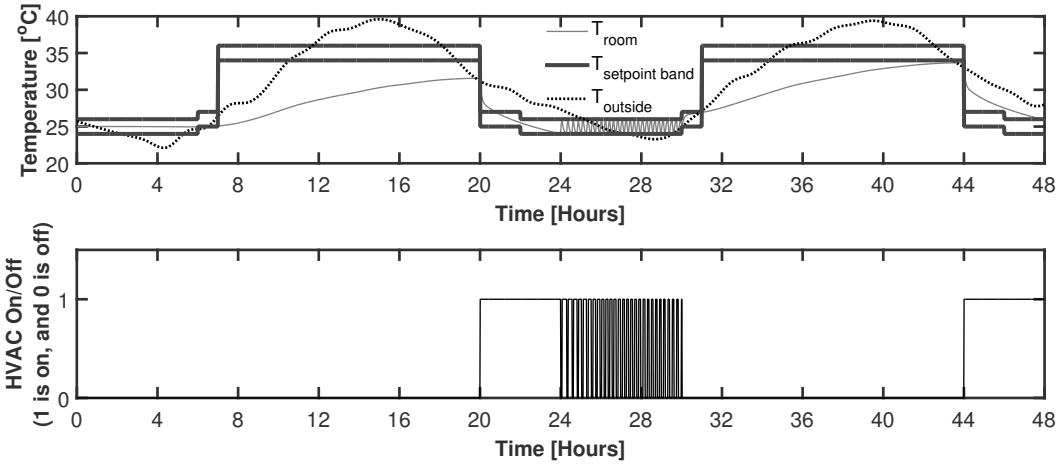


(c) MBPC method.

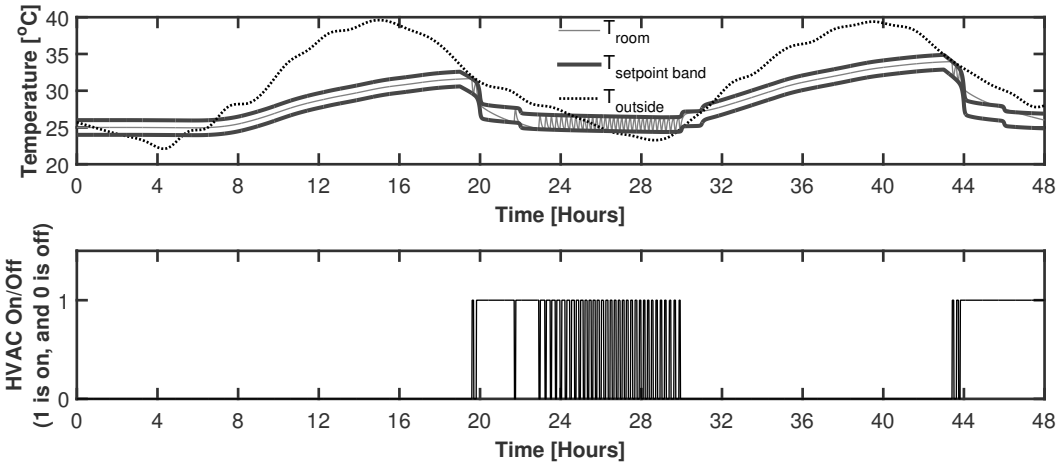


Figure 8: Simulation results of the two-story residential building model during August 1-2 in Houston, TX, showing variations of room 1's temperature and on/off status of 1000 W HVAC system using (a) the constant temperature setpoint control method; (b) the occupant-activities-based setpoint control method; and (c) the MBPC method.

in front of the receiving surface. Straightforwardly, the surface that is entirely below the receiving surface is screened out by comparing its vertical global coordinates, $z$, with those of the receiving surface. To identify the surface behind the target surface, it is required to introduce the relative coordinate system, whose origin is on the receiving surface and the z-axis is the normal direction of the receiving surface. Noted that based on this, the vertical relative coordinate, $z'$, of the flat receiving surface is always zero. The surface, whose all $z'$ components of its relative coordinate are negative, is entirely behind the receiving surface. Thereby, it can also be screen out, leaving only potential casting surfaces for further calculation.

After the potential casting surfaces are identified, the location of the shadow on the considered surface is determined by projecting the casting surface onto the receiving surface. Global coordinate $(x, y, z)$ of the clipped casting surface is projected to relative coordinate $(x', y', z')$ referenced to the receiving surface as [32]:

$$\begin{aligned} x' &= x - \frac{z \cdot a}{\cos\theta}, \\ y' &= y - \frac{z \cdot b}{\cos\theta}, \\ z' &= 0, \end{aligned} \tag{A.5}$$

where

$$\begin{aligned} a &= \sin\psi_w \sin\psi_s \sin\phi_s - \cos\psi_w \cos\psi_s \sin\phi_s, \\ b &= -\cos\psi_w \cos\phi_w \sin\psi_s \sin\phi_s - \\ &\quad \sin\psi_w \cos\phi_w \cos\psi_s \sin\phi_s + \\ &\quad \sin\phi_w \cos\phi_s. \end{aligned} \tag{A.6}$$

Note that before evaluating the shading location, part of the potential casting surface that is behind the receiving surface, identified by the relative coordinate with negative $z'$ value, is required to be clipped to avoid a pseudo-shadow.

The last step of evaluating the shading area is to calculate the overlap area of the shadow and the receiving surface. This step is done by intersecting the receiving surface with the overall shadow region, which is given by the union of all shadow regions cast from other surfaces. The shading area on the considered surface is then evaluated from the coordinates of the resulting overlap area.

## Appendix B. Ventilation and infiltration

The air mass flow rate $\dot{m}_e$ in the temperature and moisture governing equations of room air is the sum of infiltration rate $\dot{m}_i$ and ventilation rate $\dot{m}_v$. Any outdoor air that enters by way of infiltration and ventilation is assumed to be immediately mixed with the zone air. The major difference between infiltration and ventilation is that infiltration is the air exchange through the building envelopes' leakage, while ventilation is the air exchange through the opening area. For infiltration, an effective leakage area model is employed based on Sherman and Grimsrud [57]. The infiltration rate is given by

$$\dot{m}_i = 10\, A_c \sqrt{c_s \left|T_a - T_e\right| + c_w \left(V_{wind}\right)^2}, \tag{B.1}$$

where $A_c$ ($m^2$) is the effective air leakage area (taken as 2% of the total surface area of a wall) of each exterior surface; $T_a$ and $T_e$ are the room air temperature and outside temperature; $c_s$ and $c_w$ are the stack and wind coefficients, respectively, which depend on the structure's geometry. More details regarding $c_s$ and $c_w$ are found in Sherman and Grimsrud [57].

Ventilation usually occurs when a door or a window is open. In this work, only ventilation between indoor air and outdoor air is considered. According to ASHRAE [31], the ventilation rate combines both wind-driven and stack-driven effects:

$$\dot{m}_v = \sqrt{\dot{m}_s^2 + \dot{m}_w^2}, \tag{B.2}$$

where $\dot{m}_s$ is the stack-driven ventilation, and $\dot{m}_w$ is the wind-driven ventilation.

The air mass flow rate that is stack-driven is governed by the temperature difference:

$$\dot{m}_s = c_D\, A_{opening}\, F_{schedule} \sqrt{2\, g\, \Delta H_{NPL}\, \left(\left|T_a - T_o\right| / T_a\right)}, \tag{B.3}$$

where $A_{opening}$ is the surface area of the opening (i.e., window or door); $c_D$ is the discharge coefficient:

$$c_D = 0.40 + 0.0045\left|T_a - T_o\right|, \tag{B.4}$$

$\Delta H_{NPL}$ is the height from the midpoint of the lower opening to the neutral pressure level. Available data of $\Delta H_{NPL}$ in various kinds of buildings is limited. The value of $\Delta H_{NPL}$ in tall buildings varies from 0.3 to 0.7 of total building height [58]. For houses, especially houses with chimneys, $\Delta H_{NPL}$ is usually above the middle height of the building. Also note that for air ventilation between multi-zones, there is no wind-driven effect but only a stack-driven effect.

Wind-driven ventilation is primarily dependent on the wind speed:

$$\dot{m}_w = c_v A_o V_{wind}, \tag{B.5}$$

where $c_v$ is 0.5 to 0.6 for perpendicular winds and 0.25 to 0.35 for diagonal winds; $A_o$ is the opening area; $V_{wind}$ is the local wind speed.

## References


[1] D&R International, Ltd., Building energy data book, Tech. rep., U.S. Department of Energy (2009).

[2] A. I. Dounis, C. Caraiscos, Advanced control systems engineering for energy and comfort management in a building environment--a review, Renewable and Sustainable Energy Reviews 13 (6) (2009) 1246–1261.

[3] HoneyWell, retrieved September 30, 2015, from http : //yourhome.honeywell.com/home/Products/Thermostats/ (2015).

[4] Ecobee, retrieved Septemper 30, 2015, from http : //www.ecobee.com/ (2015).

[5] NEST labs: Enhanced auto schedule, retrieved September 30, 2015, from https : //nest.com/downloads/press/documents/enhanced – auto – schedule – white – paper.pdf (November 2014).

[6] A. Afram, F. Janabi-Sharifi, Theory and applications of hvac control systems–a review of model predictive control, Building and Environment 72 (2014) 343–355.

[7] P. H. Shaikh, N. B. M. Nor, P. Nallagownden, I. Elamvazuthi, T. Ibrahim, A review on optimized control systems for building energy and comfort management of smart sustainable buildings, Renewable and Sustainable Energy Reviews 34 (2014) 409–429.

[8] S. Privara, J. Cigler, Z. Váňa, F. Oldewurtel, C. Sagerschnig, E. Žáčeková, Building modeling as a crucial part for building predictive control, Energy and Buildings 56 (2013) 8–22.

[9] M. Maasoumy, A. Pinto, A. Sangiovanni-Vincentelli, Model-based hierarchical optimal control design for HVAC systems, in: ASME 2011 Dynamic Systems and Control Conference and Bath/ASME Symposium on Fluid Power and Motion Control, American Society of Mechanical Engineers, 2011, pp. 271–278.

[10] A. Aswani, N. Master, J. Taneja, D. Culler, C. Tomlin, Reducing transient and steady state electricity consumption in HVAC using learning-based model-predictive control, Proceedings of the IEEE 100 (1) (2012) 240–253.

[11] F. Oldewurtel, A. Parisio, C. N. Jones, D. Gyalistras, M. Gwerder, V. Stauch, B. Lehmann, M. Morari, Use of model predictive control and weather forecasts for energy efficient building climate control, Energy and Buildings 45 (2012) 15–27.

[12] M. H. Amini, J. Frye, M. D. Ili, O. Karabasoglu, Smart residential energy scheduling utilizing two stage mixed integer linear programming, in: North American Power Symposium (NAPS), 2015, 2015, pp. 1–6.

[13] M. Schmelas, T. Feldmann, E. Bollin, Adaptive predictive control of thermo-active building systems (tabs) based on a multiple regression algorithm, Energy and Buildings 103 (2015) 14 – 28.

[14] F. Ascione, N. Bianco, C. D. Stasio, G. M. Mauro, G. P. Vanoli, Simulation-based model predictive control by the multi-objective optimization of building energy performance and thermal comfort, Energy and Buildings 111 (2016) 131 – 144.

[15] D. B. Crawley, C. O. Pedersen, L. K. Lawrie, F. C. Winkelmann, EnergyPlus: energy simulation program, ASHRAE journal 42 (4) (2000) 49.

[16] F. Winkelmann, B. Birdsall, W. Buhl, K. Ellington, A. Erdem, J. Hirsch, S. Gates, Doe-2 supplement: version 2.1 e, Tech. rep., Lawrence Berkeley Lab., CA (United States); Hirsch (James J.) and Associates, Camarillo, CA (United States) (1993).

[17] G. Fraisse, C. Viardot, O. Lafabrie, G. Achard, Development of a simplified and accurate building model based on electrical analogy, Energy and buildings 34 (10) (2002) 1017–1031.

[18] ESP-r, retrieved July 28, 2014, from http : //www.esru.strath.ac.uk/Programs/ESP – r.htm (2011).

[19] X. Li, J. Wen, Review of building energy modeling for control and operation, Renewable and Sustainable Energy Reviews 37 (2014) 517–537.

[20] R. Kramer, J. van Schijndel, H. Schellen, Simplified thermal and hygric building models: a literature review, Frontiers of Architectural Research 1 (2012) 318–325.

[21] A. Foucquier, S. Robert, F. Suard, L. Stephan, A. Jay, State of the art in building modelling and energy performances prediction: A review, Renewable and Sustainable Energy Reviews 23 (2013) 272–288.

[22] N. Yu, S. Salakij, R. Chavez, S. Paolucci, M. Sen, P. Antsaklis, Model-based Predictive Control for Building Energy Management II: Experimental Validations, To be submitted to Energy and Buildings.

[23] Revit Architecture, AutoDesk, retrieved February 16, 2016, from http : //www.autodesk.com/products/revit – family/overview (2013).

[24] M. Gouda, S. Danaher, C. Underwood, Building thermal model reduction using nonlinear constrained optimization, Building and Environment 37 (12) (2002) 1255–1265.

[25] O. T. Ogunsola, L. Song, Review and evaluation of using rc thermal modeling of cooling load prediction for hvac system control purpose, in: ASME 2012 International Mechanical Engineering Congress and Exposition, American Society of Mechanical Engineers, 2012, pp. 735–743.

[26] A. P. Ramallo-GonzAlez, M. E. Eames, D. A. Coley, Lumped parameter models for building thermal modeling: An analytic approach to simplifying complex multi-layered constructions, Energy and Buildings 60 (2013) 174–184.

[27] F. Tariku, K. Kumaran, P. Fazio, Integrated analysis of whole building heat, air and moisture transfer, International Journal of Heat and Mass Transfer 53 (15) (2010) 3111–3120.

[28] R. B. Bird, W. E. Stewart, E. N. Lightfoot, Transport Phenomena, John Wiley & Sons, 2006.

[29] T. Shemmeri, Building's heat gain, Tech. rep., Staffordshire University (2011).

[30] US Department of Energy, Input and Output Engineering Reference of EnergyPlus (2012).

[31] R. Parsons, R. Parsons, C. Forman, ASHRAE handbook-fundamentals, American Society of Heating, Refrigerating and Air Conditioning Engineers, Inc., ip édition, 1989.

[32] Lawrence Berkeley National Laboratory, Berkeley, CA, EnergyPlus Documentation, Engineering Reference: The Reference to EnergyPlus Calculation (2013).

[33] J. Bear, Y. Bachmat, Introduction to modeling of transport phenomena in porous media, Kluwer Academic, New York, 1990.

[34] J. H. Klems, U-values, solar heat gain, and thermal performance: Recent studies using the MoWiTT, Lawrence Berkeley Laboratory, 1988.

[35] S. Saneinejad, P. Moonen, T. Defraeye, J. Carmeliet, Analysis of convective heat and mass transfer at the vertical walls of a street canyon, Journal of Wind Engineering and Industrial Aerodynamics 99 (4) (2011) 424–433.

[36] H. M. Knzel, Simultaneous heat and moisture transport in building componentsone-and two-dimensional calculation using simple parameters, Ph.D. thesis, IRB Verlag, Fraunhofer-Informationszentrum Raum and Bau, Stuttgart, Germany (1995).

[37] M. Janz, B. F. Johannesson, Measurement of the moisture storage capacity using sorption balance and pressure extractors, Journal of Building Physics 24 (4) (2001) 316–334.

[38] F. Tariku, K. Kumaran, P. Fazio, Transient model for coupled heat, air and moisture transfer through multilayered porous media, International Journal of Heat and Mass Transfer 53 (15) (2010) 3035–3044.

[39] T. Horikawa, D. D. Do, D. Nicholson, Capillary condensation of adsorbates in porous materials, Advances in colloid and interface science 169 (1) (2011) 40–58.

[40] A. Bejan, Convection Heat Transfer, John Wiley and Sons, 1984.

[41] J. A. W. Elliott, On the complete Kelvin equation, Chemical Engineering Education 35 (4) (2001) 274–279.

[42] H. M. Künzel, A. Holm, D. Zirkelbach, A. N. Karagiozis, Simulation of indoor temperature and humidity conditions including hygrothermal interactions with the building envelope, Solar Energy 78 (4) (2005) 554–561.

[43] F. Tariku K. Kumaran, P. Fazio, Transient model for coupled heat, air and moisture throughmultiplayered porous media, International Journal of Heat and Mass Transfer 53 (2010) 3035–3044.

[44] M. O. Abadie, K. C. Mendiaca, Moisture performance of building materials: From material characterization to building simulation using the moisture buffer value concept, Building and Environment 44 (2009) 388–401.

[45] S. Wilcox, M. W., Users Manual for TMY3 Data Sets, National Renewable Energy Laboratory (2008).

[46] P. J. Roache, Fundamentals of verification and validation, Hermosa Publ., 2009.

[47] E. J. Davison, A method for simplifying linear dynamic systems, Automatic Control, IEEE Transactions on 11 (1) (1966) 93–101.

[48] E. Davison, Further remarks on simplifying linear dynamic systems, Automatic Control, IEEE Transactions on 12 (2) (1967) 213–214.

[49] E. Davison, Further comments on" a method for simplifying linear dynamic systems", Automatic Control, IEEE Transactions on 12 (6) (1967) 799–800.

[50] B. Moore, Principal component analysis in linear systems: Controllability, observability, and model reduction, IEEE Transactions on Automatic Control 26 (1) (1981) 17–32.

[51] D. Kim, J. Braun, Reduced-order building modeling for application to model-based predictive control, in: Fifth national conference of IBPSA-USA, Madison, WI, 2012, pp. 1,2.

[52] R. Bualan, J. Cooper, K.-M. Chao, S. Stan, R. Donca, Parameter identification and model based predictive control of temperature inside a house, Energy and Buildings 43 (2) (2011) 748–758.

[53] M. Georgescu, I. Mezi, Building energy modeling: A systematic approach to zoning and model reduction using koopman mode analysis, Energy and Buildings 86 (2015) 794–802.

[54] D. Kim, J. Braun, E. Cliff, J. Borggaard, Development, validation and application of a coupled reduced-order {CFD} model for building control applications, Building and Environment 93, Part 2 (2015) 97 – 111.

[55] M. Aoki, Control of large-scale dynamic systems by aggregation, Automatic Control, IEEE Transactions on 13 (3) (1968) 246–253.

[56] B. D. Anderson, J. B. Moore, Optimal control: linear quadratic methods, Courier Corporation, 2007.

[57] M. H. Sherman, D. T. Grimsrud, Infiltration-pressurization correlation:

Simplified physical modeling, ASHRAE Transactions 86 (2) (1980) 778–803.

[58] G. T. Tamura, A. Wilson, Pressure differences for a nine-storey building as a result of chimney effect and ventilation system operation, ASHRAE Transactions 72 (1) (1966) 180–189.